Nucleation of nanodiamonds in H-atom rich microplasma

Abdoulaye Constant Siby, Arvind K Bhakta, Joel Jeevan, Xiaonan Sun, Philippe Decorse, Souad Ammar, Khaled Hassouni, Swaminathan Prasanna

Carbon

Nucleation of nanodiamonds in H-atom rich microplasma

--Manuscript Draft--

Manuscript Number:	CARBON-D-24-03795
Article Type:	Research Paper
Keywords:	Nanodiamonds, Nucleation, MW plasma,
Corresponding Author:	Swaminathan Prasanna Laboratory of Science of Processes and Materials FRANCE
First Author:	Abdoulaye Constant Siby
Order of Authors:	Abdoulaye Constant Siby
	Arvind Kumar Bhakta
	Joel Jeevan
	Xiaonan Sun
	Philippe Decorse
	Souad Ammar
	Khaled Hassouni
	Swaminathan Prasanna
Abstract:	In this study, the formation and properties of carbon nanostructures obtained from a low-pressure-low temperature microplasma operated with H$_2$/CH$_4$ gas precursors were investigated. The study reveals gas phase nucleation of nanodiamonds among other phases of carbon such as graphite and amorphous carbon. Raman spectroscopy revealed that the signature of the nanostructures produced was insensitive to the nature of the substrate. The main conclusion of the paper is that nucleating of nanodiamonds is sustained by high densities of H-atoms at moderate gas temperatures and optimum concentrations of hydrocarbon radicals and molecules. High densities of hydrocarbons push the equilibrium towards sp^2 and amorphous nanostructures even under high H-atom densities.
Suggested Reviewers:	Sergey Baryshev Michigan State University serbar@msu.edu
	Kazuo Terashima kazuo@plasma.k.u-tokyo.ac.jp
	Amanda Barnard Amanda.S.Barnard@anu.edu.au
Opposed Reviewers:	

This piece of the submission is being sent via mail.

Dear Editor

We would like to submit our paper titled “Nucleation of nanodiamonds in H-atom rich microplasma” for peer review in your journal.
The paper focusses on understanding the conditions that allow for formation of nanodiamonds in a moderate pressure plasma. Extensive characterization of materials with characterization of plasma conditions allows to deduce these operating conditions conducive for the nucleation of nanodiamonds.
We believe that the paper addresses key issues that allign with the scope of the journal and the interests of the audience of the journal.
We would be happy if you consider our paper for evaluation through peer review process.

With best regards
Swaminathan Prasanna
LSPM CNRS
Villetaneuse France

CARBON Submission Checklist

Please check the following points before approving the pdf file for your manuscript. **Manuscripts that do not conform may be returned for correction and resubmission.** You should be able to answer "yes" to all the following questions. Items 11 and 14 may not be applicable.		
1.	**FONT/SPACING:** Is the manuscript double–spaced or 1.5-spaced with a font size of 12pt? **Note**: Times or New Times Roman preferred.	Yes
2.	**CO-AUTHORS:** Have you given full addresses and affiliations for all co–authors?	Yes
3.	**ABSTRACT:** Does the manuscript include a one paragraph abstract of less than 200 words (Review articles and Research papers) or less than 100 words (Letters)? **Note**: Make sure the abstract is included in the manuscript. For the manuscript of a Letter separate the abstract from the text by an extra line space or a horizontal line.	Yes
4.	**CORRESPONDING AUTHOR:** Is the corresponding author or corresponding authors identified by * and contact details (email address) given as a footnote to the first page? Do not include the address, which should be included in the manuscript heading as part of the author affiliations. Use the following format: * Corresponding author. *EXAMPLE: E-mail address:* mut11@psu.edu (Mauricio Terrones). **Note**: Carbon allows more than one corresponding author to be listed on the manuscript. During submission, however, the electronic system will request a single corresponding author with whom we will communicate during the review purposes. **This should be the lead author.**	Yes
5.	**REGULAR RESEARCH PAPERS:** Have you a Methodology/Experimental section? Are the sections ordered according to the journal style? 1. Introduction 2. Methodology/Experimental 3. Results and Discussion 4. Conclusion	Yes
6.	**SECTIONS-NUMBERING:** Are sections given Arabic numbers with subsections numbered using the decimal system? For example: 2. Experimental 2.1 Sample preparation 2.1.1 Sample modification **Note**: Acknowledgements and References sections are not numbered.	Yes
7.	**REFERENCES:** • Are they each given a different number? (do not use 14a. b. c., *etc*.) • Do they all include manuscript titles, volume and page range? • Have you given the first six author names followed by *et al.*? • Are they accessible and archival?	Yes

	Note: "Web pages, private communications, unpublished results, etc. should be given as footnotes."	
8.	**SYMBOLS/LINKS:** Are all symbols and document links replicated correctly in the pdf file?	Yes
9.	**CAPTIONS:** Do figure and table captions appear on the same page as the item they describe? **Note**: Figures and tables should appear after the text where they are introduced.	Yes
10.	**FIGURES:** Have you designated all illustrative items as "Figures"? **Note**: Charts, diagrams, schemes and photographs are all to be referred to in CARBON as "Figures".	Yes
11.	**CARBON ABBREVIATION:** Have you included the carbon in abbreviations (CNT, CNF, MWCNT, *etc.*)? **Note**: English grammar dictates that the abbreviation must refer to the singular. One does not use the plural noun as an adjective (*e.g.*, fiber composites, fruit salad, nanotube dimensions, vegetable soup, *etc.*). One may say "the production of MWCNTs", but writes "MWCNT production", "MWCNT properties", *etc*.	No
12.	**LETTER TO THE EDITOR:** Is the text, including references, less than five double-spaced pages with not more than five tables and figures combined?	Yes
13.	**REVIEWERS:** Have you recommended at least three internationally recognized peer reviewers from at least two different countries? **Note**: Recommendations should include full names, email addresses and a short rationale for the suggested reviewer choice.	Yes
14.	**ABBREVIATIONS:** Does your use of abbreviations conform to the following guidelines? 1. To define an abbreviation, first write the term in full followed by the abbreviation in parentheses. "X-ray diffraction (XRD) examination showed that the samples were ….." Do not do the reverse. 2. Never use or define an abbreviation in the manuscript title. 3. Never use abbreviations in the Abstract without defining them, and only define them if they are used later in the Abstract. 4. Define an abbreviation the first time it is used in the text, even though it may also have been necessary to define it in the Abstract. 5. Only define an abbreviation if you are going to use it later.	Yes
15.	**RESUBMISSIONS:** If this is a resubmission as a result of comments from the Editor-in-Chief, *i.e.* generally before peer review, have you included replies to these comments in your cover letter?	
16.	**GRAPHICAL ABSTRACT:** Have you included a Graphical Abstract, as specified by Elsevier (https://www.elsevier.com/authors/journal-authors/graphical-abstract)?	Yes

Graphical Abstract

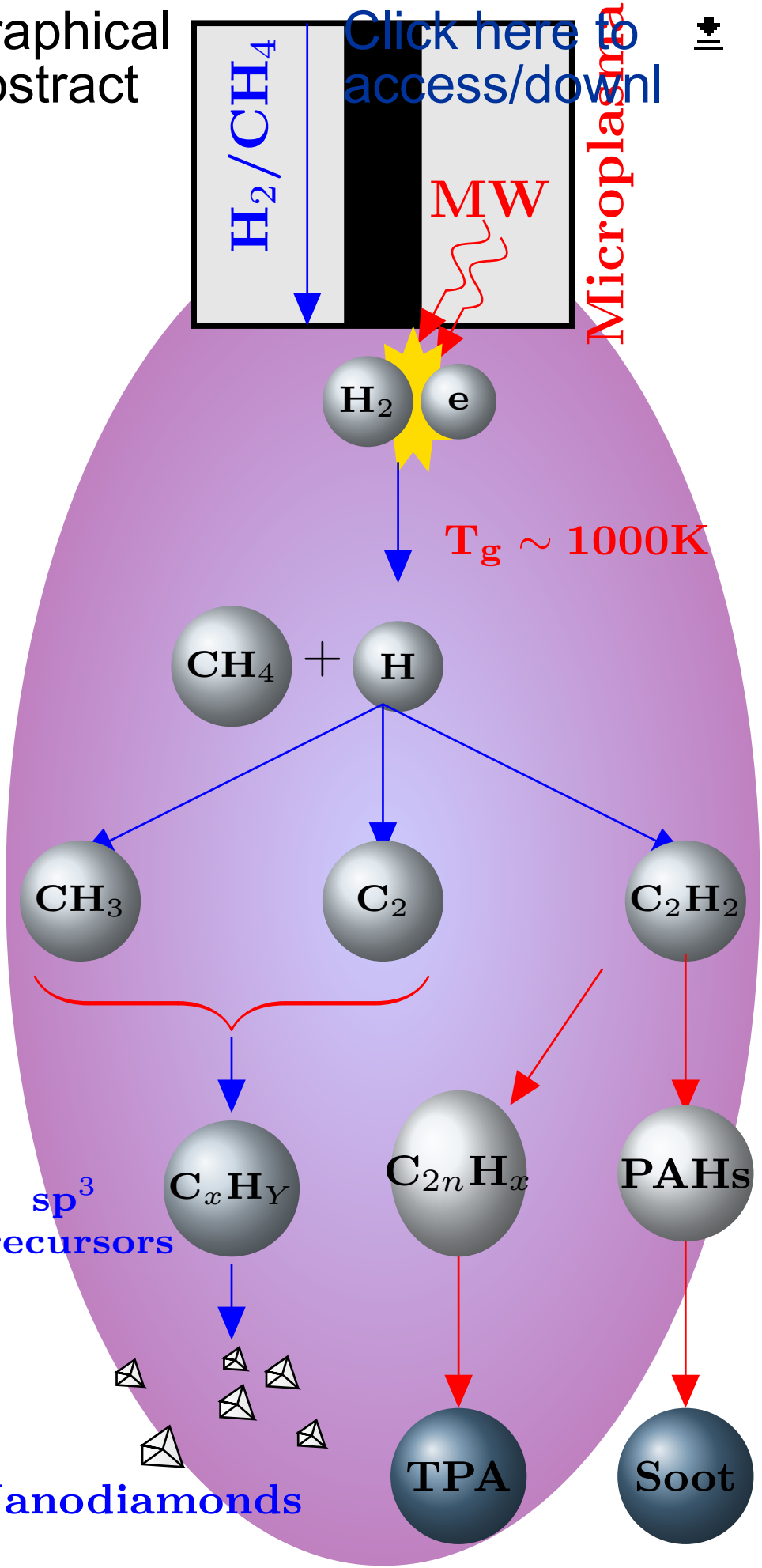

Graphical Abstract

Nucleation of nanodiamonds in H-atom rich microplasma

Abdoulaye Siby, Arvind Bhakta, Joel Jeevan, Xiaonan Sun, Philippe Decorse, Souad Ammar, Khaled Hassouni, Swaminathan Prasanna

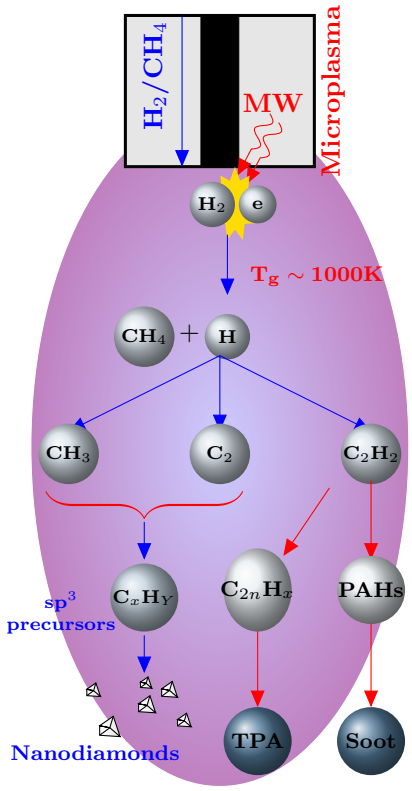

Highlights

Nucleation of nanodiamonds in H-atom rich microplasma

Abdoulaye Siby, Arvind Bhakta, Joel Jeevan, Xiaonan Sun, Philippe Decorse, Souad Ammar, Khaled Hassouni, Swaminathan Prasanna

- Gas phase nucleation of diamond nanoparticles at low temperature low pressure conditions
- H-atom rich and moderate temperatures are key to sp^3 molecular growth and nucleation
- High-densities of hydrocarbons tilt the balance towards growth of soot and transpolyacetylene.

Nucleation of nanodiamonds in H-atom rich microplasma

Abdoulaye Siby[a], Arvind Bhakta[a], Joel Jeevan[a], Xiaonan Sun[b], Philippe Decorse[b], Souad Ammar[b], Khaled Hassouni[a], Swaminathan Prasanna[a,*]

[a] *LSPM CNRS, UPR 3407, Universite Sorbonne Paris Nord, 99 avenue J.B. Clément, 93430, Villetaneuse, France*
[b] *Universite Paris Cite, CNRS UMR-7086, ITODYS, 15 Rue Jean-Antoine de Baif, 75251, Paris, France*

Abstract

In this study, the formation and properties of carbon nanostructures obtained from a low-pressure-low temperature microplasma operated with H_2/CH_4 gas precursors were investigated. The study reveals gas phase nucleation of nanodiamonds among other phases of carbon such as graphite and amorphous carbon. Raman spectroscopy revealed that the signature of the nanostructures produced was insensitive to the nature of the substrate. The main conclusion of the paper is that nucleating of nanodiamonds is sustained by high densities of H-atoms at moderate gas temperatures and optimum concentrations of hydrocarbon radicals and molecules. High densities of hydrocarbons push the equilibrium towards sp^2 and amorphous nanostructures even under high H-atom densities.

Keywords: keyword one, keyword two

PACS: 0000, 1111

2000 MSC: 0000, 1111

1. Introduction

Nucleation of diamond phase of carbon is one of the most fascinating questions that has intrigued scientists for ages, owing to its lower theromodynamic

*Corresponding author
Email address: swaminathan.prasanna@lspm.cnrs.fr (Swaminathan Prasanna)

stability with respect to the sp^2 hybridized graphite structure of carbon. The sp^3 hybridized diamond phase is only stable at high pressures and high temperatures, and can exist at room temperature due to super-cooling from these extreme conditions. Natural diamond from Earth's crust or the interstellar grains of diamond reteived from meteorites are formed because of extreme conditions conducive to nucleation of diamonds. On a laboratory scale, many processes such as detonation[1], laser ablation [2, 3], ultrasound cavitation [4], HPHT process [5, 3, 6] and cold compression synthesis [7] have demonstrated producing diamond from nanometric to mircometric sizes. These methods depend on generating extreme temperature and pressure conditions, where the diamond form is more stable than the graphite form, followed by rapid cooling to significantly lower temperatures to prevent the diamond phase from transitioning into the more stable graphite phase.

Heterogeneous nucleation or growth of diamond over diamond seeds through chemical vapor deposition (CVD) at moderate pressure and low temperature conditions is well established in the laboratory. CVD diamonds have been commercialized for applications ranging from jewelry and machine tools to advanced applications in biotechnology, electronics, and quantum computing. In a moderate pressure plasma ($\sim$ 100 mbar) CVD process, the growth of diamond occurs through heterogeneous growth that is driven by surface stabilization offered by the substrate [8, 9, 10]. The process proceeds through (i) the attachment of carbon radicals such as methyl (CH_3)[11] or C_2[12] to nucleation sites on diamond seeds and (ii) the subsequent conversion of unstable sp^1 and sp^2 bonds in the presence of etchant such as atomic-H, resulting in a stable sp^3 phase. The role of atomic-H is essentially to prevent the dangling bonds on the diamond surface from forming carbon double bonds, thus avoiding graphitization of the diamond surface and, therefore, stabilizing the diamond phase. Moreover, the attachment of carbon radicals such as methyl ensures maintaining sp^3 hybridized states. Further, the hydrogen atoms of the attached radical are involved in adsorption/recombination equilibrium with gas phase H-atom, which dynamically generates new active sites where the gas-phase radicals can be attached. This is

the reason why seeding the surface with nanodiamond particles becomes critical for the growth of CVD nanocrystalline or polycrystalline diamonds [9].

The traditional methods of producing nanodiamonds required for CVD growth usually come from (i) detonation[1] and (ii) milling of natural or High Pressure High Temperature (HPHT) diamond[3]. Furthermore, the remarkable properties of nanodiamonds have extended their applications across a broad spectrum of fields in biomedical, electronics, and quantum technologies[13, 3, 14]. However, these applications that demand consistent and long photoluminescence time require DNPs with a low surface sp^2 coverage, a homogeneous distribution of the dopant and a narrow size distribution around 10 nm. Unfortunately, these requirements remain the main bottlenecks of the extended application of DNPs as traditional methods for their production, such as (i) detonation[1] and (ii) milling of natural or High Pressure High Temperature (HPHT) diamond[3] suffer from large distributions of particle sizes, poor crystalline quality, high impurities and non-homogeneous distribution of dopants[13, 3, 1]. This makes it necessary to introduce additional complex and time-consuming purification steps. It has been recognized that bottom-up production strategy can be well suited to meet these specific demands as the DNPs, pure and doped, are nucleated from a careful selected mixture of hydrocarbon and dopant precursors[13].

It was generally thought that gas phase nucleation of diamond at softer metastable conditions is not feasible. Although the formation of interstellar diamonds is often linked to extreme occurrences like supernova explosions, ample evidence exists supporting the nucleation of hydrocarbons in interstellar gas under low-pressure conditions [15, 16, 17]. However, there have been several studies that demonstrate diamond of nanometric sizes could also be nucleated in gas phase at low-pressure and low temperature conditions in the laboratory plasmas. Several recent investigations have demonstrated the homogeneous nucleation of DNPs in the plasma gas phase using a diverse range of hydrocarbon precursor gases, including methane[18, 19, 20], ethanol, [21, 22], halogenated hydrocarbons, [23, 24], and others. The major difference between the growth of CVD diamond and the homogeneous nucleation of nanodiamonds is that CVD

diamond synthesis mainly focuses on the crystal growth on pre-existing micro-seeds, the gas phase nucleation of sp^3 nanostructures would proceed through formation of the intermediate sp^3 molecules that grow and nucleate as nanodiamonds. Unfortunately, there is lack of identification of these intermediate molecules and therefore, understanding of the molecular growth and nucleation processes. Consequently, despite the experimental evidence supporting the homogeneous nucleation of nanodiamonds, this phenomenon is frequently met with doubt.

In this work, we extend the study of Jia et al. [19] to probe the mechanism and conditions leading to the nucleation of nanodiamonds. Substantial amounts of DNP were shown to be produced at 100 mbar and a power of 90 W for a gas mixture of 4% CH_4/H_2. These DNPs were embedded in a composite containing graphitic and amorphous carbon. It was demonstrated that the local plasma conditions, namely the electron density, gas temperature, and H-atom density, must play a pivotal role on nucleation, growth, and crystallinity of nanodiamonds. On the other hand, it was identified that hydrocarbon radicals C_2 and CH_3 could have a significant role in the molecular growth of sp^3 molecules that lead to the nucleation of DNPs. Further exploration of the impact of H-atom and hydrocarbon on the nucleation density, growth rate, and quality of nanodiamonds produced has been undertaken in the present work. The research methodology involves a combination of plasma diagnostics and material characterization to obtain improved insights on the mechanism leading to the nucleation of nanodiamonds and to ascertain the optimum conditions to have the maximum yield of nanodiamonds. The morphology of the carbon nanostructures produced as a function of pressure and methane concentration are correlated with the plasma diagnostics. The experimental setup used for the collection of carbon nanostructures is discussed in Section 2. In Section 3, the characterization of carbon nanostructures is correlated with the deposition conditions and finally we present the systematic study to decipher the competition between surface and gas phase processes in Section 4 and try to identify the conditions conducive to nucleate nanodiamonds.

2. Experimental set-up

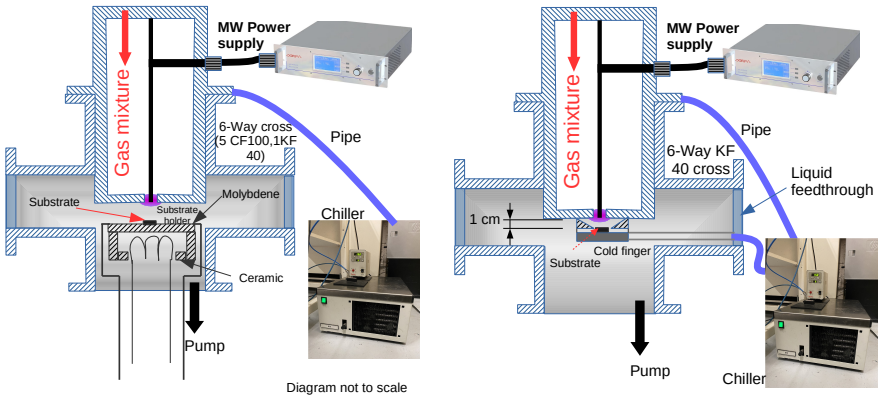

(a) Heating/bias system (b) Cold-finger sytstem

Figure 1: Experimental set-up for carbon particle deposition using the MW microplasma torch

The details of the MW torch used to produce DNPs have been provided in [19]. Experiments were carried out at a constant power of 90W where it was shown maximum yield of nanodiamond at 100 mbar [19]. In this study, the pressure range was extended between 75 and 125 mbar to explore the influence of pressure and methane concentration on the morphology of carbon nanostructures. The carbon nanostructures formed with the microplasma operated with H_2/CH_4 gas precursors were collected downstream on a substrate. Two different systems were used to collect the carbon nanostructures and their schematic have been provided in Figure 1. The two collection systems allows for changing the local conditions at the substrate surface such as polarization, temperature, distance and therefore permits investigation of plasma surface interaction or collection of dusts formed in the plasma.

The first system allows for polarizing or heating the substrate. The reactor is basically a 6 way cross whose 5 flanges are CF 100 while the last flange is a KF40 flange that was used to attach the microplasma torch. The substrate holder was placed directly below the torch. The substrate holder was composed of a sandwich of molybdenum disc, graphite heater, and an alumina cup. The

temperature of the substrate was measured using a thermocouple just beneath the molybdenum disc. The ceramic cup was placed on a stainless steel tube. This design of the substrate holder provided flexibility with respect to modifying the discharge conditions by heating to temperatures up to 500 ^oC as well as positive/negative polarization. Furthermore, the distance between the substrate holder and the torch can be changed. The particles were collected on a substrate such as silicon or fiberglass placed on the substrate holder downstream of the plasma torch. This deposition system is schematically illustrated in Figure 1a. This experimental setup shows the elements of the vacuum system (gauge, pump), the torch, and a 200 W Sairem microwave generator at 2.45 GHz (GMP20). Unless otherwise specified, most of the deposition experiments have been performed using this reactor.

The second system allows for cooling the substrate and allows for studying substrate conditions that was not achievable with the first system. The reactor was basically a 6-way KF40 cross whose one arm was dedicated to the microplasma torch. The particles are collected on a substrate placed on a water-cooled substrate holder placed directly below the torch (Figure 1b). In this configuration, the distance between the substrate and the plasma torch is fixed at 1 cm. The upper part of the substrate holder is a conical nozzle that forces the gas discharge onto the substrate placed on the cold-heat exchanger made of copper. Cold water from a chiller is circulated in the heat exchanger through liquid feed-through.

3. Characterization of carbon nanostructures

All the experiments were performed on pristine substrates without any pretreatment or seeding. We rely on different complementary techniques to characterize the carbon nanostructures as presented in Table 1.

The carbon nanostructures collected on the substrate could be visually observed for most conditions. Energy dispersive X-ray spectroscopy (EDX) revealed that the observed nanostructures are mainly composed of carbon (C),

Technique	Characterization
Raman	Analysis of molecular structure, identification of chemical bonds and crystalline phases (sp^2, sp^3)
XPS	Surface chemical composition and chemical bonding analyses.
AFM/ SEM	Surface morphology/ particles size distribution.
TEM	Analysis of crystalline structure of nanoparticles

Table 1: Characterization of carbon nanostructures

with minor traces of oxygen (O) and silicon (Si). These impurities are likely due to contamination of the substrate during characterization. The characterization of the material through SEM, TEM, and AFM indicated the deposition of agglomerated nanostructures. Figure 2 shows the characteristics of the carbon nanostructures examined using AFM, synthesized at a power of 90 W at 100 mbar and 4% methane. The particle size distribution of DNPs obtained using AFM is consistent with a log-normal distribution with a mean diameter of 13.63 nm.

It was also possible to detect diamond phase in carbon nanostructures collected directly on a carbon TEM grid placed in the cold finger for about 5 minutes. TEM images and electron diffraction of this deposit are shown in Figure 2c. The TEM image shows aggregates of carbonaceous nanostructures with particle size on the order of a few nanometers, as indicated by the 20 nm scale. The associated electron diffraction image shows a characteristic diffraction pattern with concentric rings, indicating the presence of nanocrystals within the amorphous matrix. The diffraction rings suggest the presence of a crystalline diamond with orientations (111) and (220). This information corroborates the hypothesis that the DNPs are nucleated in the gas phase.

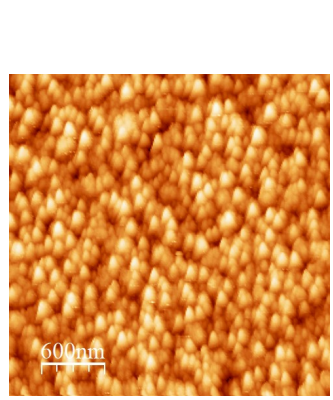

(a)

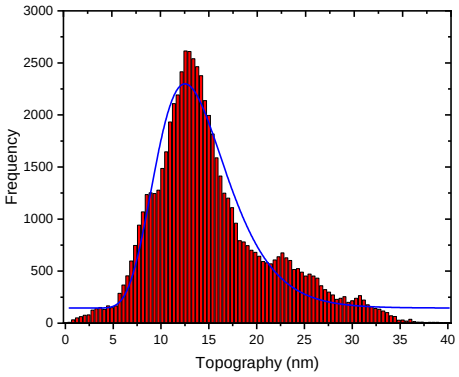

(b)

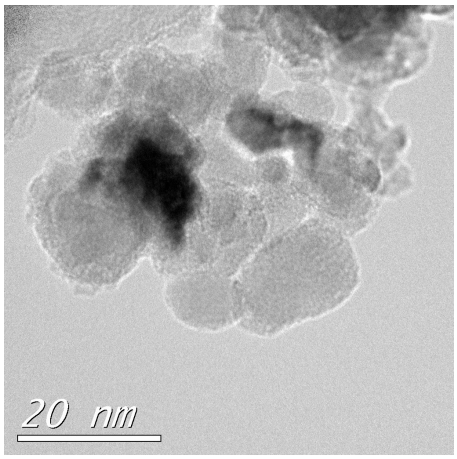

(c) TEM image

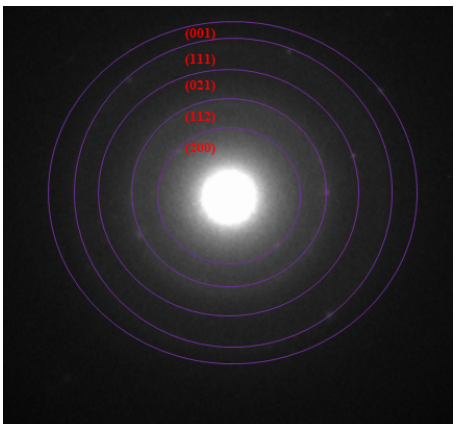

(d)

Figure 2: (a) AFM image and its corresponding (b) particle size distribution after 60 min of deposition on a silicon substrate. (c) TEM image and (d) its corresponding selected area electron diffraction of carbon nanoparticles deposit for 5 min of deposition in the cold finger. Experimental conditions: $CH_4 = 4$ sccm, $H_2 = 96$ sccm, reactor pressure = 100 mbar, absorbed power = 90 W)

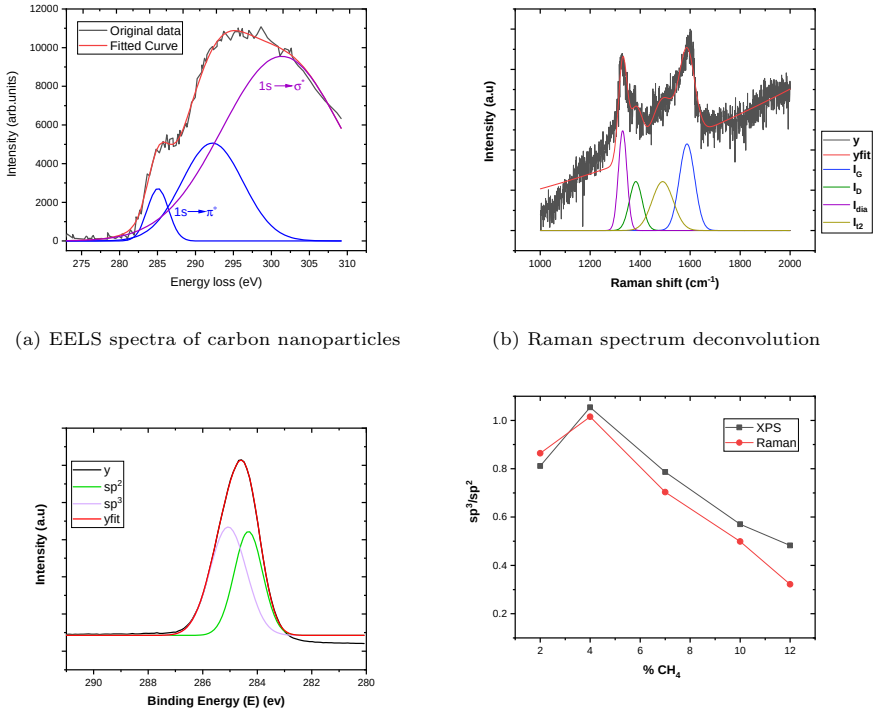

(a) EELS spectra of carbon nanoparticles

(b) Raman spectrum deconvolution

(c) Deconvolution of XPS C1s line to sp^3/sp^2 configuration

(d) Variation of the sp^3/sp^2 ratio as a function of methane concentration measured by XPS (black) and Raman (red).

Figure 3: and (c) EELS spectra of carbon nanoparticles deposit for 5 min of deposition in the cold finger. Experimental conditions: CH_4 = 4%, Pressure = 100 mbar, power = 90W, distance plasma-substrate = 1cm.

3.1. Quality of nanodiamonds

The quality of deposited nanodiamonds can be described by the sp^3/sp^2 hybridization ratio. A high proportion of sp^3 bonds is characterized by a high ratio, characteristic of diamond. However, a low ratio indicates the presence of a high proportion of sp^2 bonds. The abundance of sp^2 and sp^3 can be accessed using electron energy loss spectroscopy (EELS) spectra, Raman and XPS.

Electron energy loss spectroscopy (EELS) spectra of carbon nanostructures are presented in Figure 3a. Two important peaks are observed in the spectrum: the π^* peak at about 285 eV, corresponding to sp^2-hybridized carbon, and

ν cm^{-1}	Peak	Characteristics
1585	I_G	**G-Band**: Represents the E_{2g} phonon of sp^2 carbon domains, signifying the presence of planar graphitic carbon.
1350	I_D	**D-Band**: Indicative of disordered sp^2 carbon structures, commonly associated with defects and disorder in the graphite lattice such as polycyclic aromatic compounds that can be regarded as precursors to graphene like carbon[25].
1332	I_{Dia}	**Diamond**: this peak is typically sharp in high-quality bulk diamonds. The presence of small nanodiamond particles leads to asymmetrical broadening of the peak [26, 27, 28, 29].
1130	I_{t1}	**Transpolyacetylene (μ_3 mode)**: Associated with the transpolyacetylene chains (C-H in plane bending) μ_3 vibrational mode [30, 31, 32].
1480	I_{t2}	**Transpolyacetylene (μ_1 mode)**: associated with the transpolyacetylene chains (C=C stretch) μ_1 vibrational mode [30, 33, 34]

Table 2: Prominent spectral features observed in the raman spectra of carbon nanostructures collected.

the σ^* peak at about 290 eV, corresponding to sp^3-hybridized carbon. This shows that the manufactured nanostructures contain a mixture of sp^2 and sp^3 hybridized carbon, reinforcing the hybrid nature observed in the TEM analysis.

The presence of small nanodiamond particles can lead to broadening and overlapping of peaks in the Raman spectra. This means that the data is not easy to interpret, and special attention was given to fitting the raw Raman data with the different peaks. A typical Raman spectrum obtained for the carbon nanostructures are shown in Figure 3b along with the deconvolution of major Raman bands as listed in Table 2. The evaluation of the sp^3/sp^2 ratio can be determined by comparing the intensities of the diamond peak (I_{dia}) and those of the non-diamond bands i.e. $I_{non-dia} = I_G + I_D + I_{t1} + I_{t2}$ from the Raman spectra. Simultaneously, the degree of amorphization is assessed by the ratio

of intensities of the D band (I_D), transpolyacetylene (I_{t1}) to the G band (I_G). Finally, the percentage of sp^3 can be determined from

$$\%sp^3 = 100\frac{60I_{dia}}{60I_{dia} + \sum I_{non-dia}} \quad (1)$$

with a signal correction factor of 60 to account for the dominant reponse of non-diamond carbon peaks to the 473 nm laser used for Raman excitation [35].

Lastly, XPS being a surface based method and that the nanostructures are no more than a few nanometers should enable quantification of the sp^3/sp^2 ratio. Figure 3c illustrates the fitting of the C1s peak with component peaks for sp^3 and sp^2 located at 285.4 and 284.5 eV respectively. Since the sensitivity factor in XPS is not affected by the chemical state of the atoms [36], the relative fraction of each carbon component (sp^2 and sp^3) was calculated based on the integrated areas under the respective peaks. Figure 3d shows the variation of the sp^3/sp^2 ratio as a function of CH_4 concentration (% CH_4) at 100 mbar and 90W power deduced from Raman spectroscopy and XPS measurements. Both techniques show a similar overall trend and therefore, Raman technique was used extensively to evaluate the abundance of diamond phase in the carbon nanostructures.

3.2. Abundance of sp^3 phase with plasma conditions

The quality of the diamond has been accessed through the content of sp^3 (I_{dia}), amorphous-disordered (I_D) and transpolyacetylene I_{trans} with respect to G-band of the carbon nanostructures function of pressure (75 to 125 mbar) and methane concentration (0 to 12%) as shown in Figure 4. The highest sp^3/sp^2 ratio, is observed at 4% methane concentration and a pressure of 100 mbar. In contrast, this optimum point is also marked by the lowest I_D/I_G ratio as well as I_{trans}/I_G. This corresponds to a more crystalline diamond with the least amorphous carbon. The results are indicative of several parallel channels of molecular growth and nucleation of carbon nanostructures. The optimum condition should be a reflection of a perfect balance between the availability of the carbon atoms needed to form substantial quantities of sp^3 hybrdized

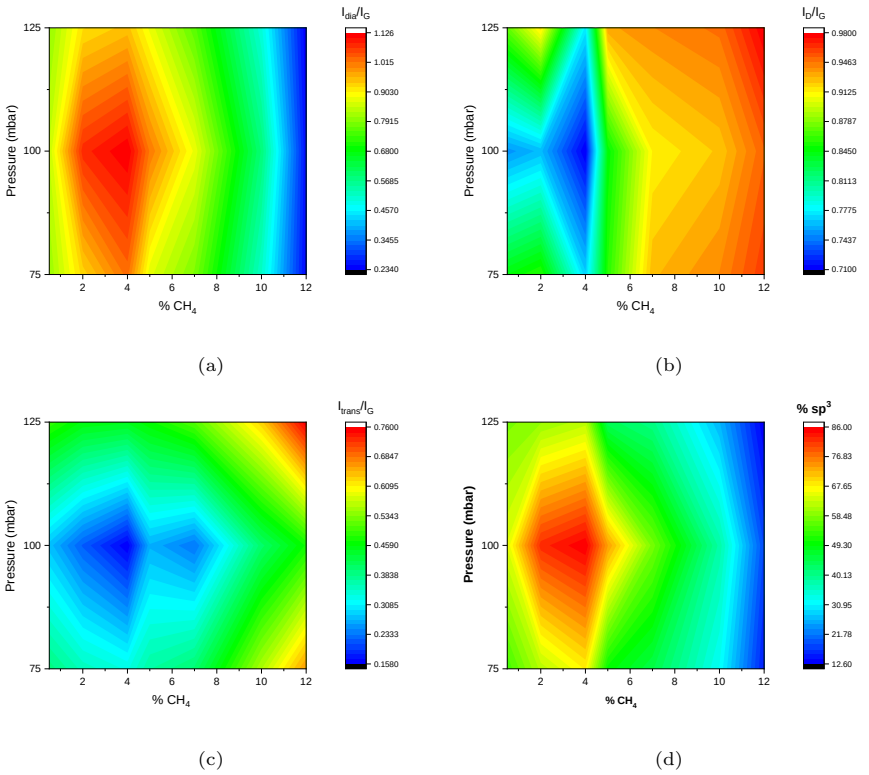

Figure 4: Distribution of (b) sp^3/sp^2 ratio and (c) I_D/I_G ratio as a function of pressure and methane concentration. Experimental conditions: Pressure = 100 mbar, injected power = 90 W, substrate = silicon, distance plasma-substrate = 1cm and deposition time = 1h.

carbon and H-atom that saturate the sp and sp^2 bonds that may have been formed, leading to maximum nucleation of nanodiamonds among other carbon nanostructures. As discussed in our previous paper [37], substantial amount of H-atoms were found even in cold regions downstream (about 1 cm away) from the plasma and is likely to saturate the molecular structures and therefore, stabilize sp^3 structures and even nanodiamonds.

The amount of carbon nanostructures collected clearly increased with methane concentration. While large deposits of carbon nanostructures were deposited for 10% of CH_4 after just 5 minutes of collection to permit easy characterization using Raman, the plasma containing 1% CH_4 produced hardly any carbon

nanostructures even after 1 hour of collection and around the inner region. This increase is simply due to the increased availability of carbon in terms of radicals such as CH_3, C_2 and reactive molecules such as C_2H_2. Unfortunately, an increase in the amount of methane seems to promote the formation of undesirable nanostructures, reducing the quality of synthesized nanodiamonds. This can be confirmed by the I_D/I_G ratio, which increases substantially with increase in CH_4 concentration. Irrespective of the pressure regime, three distinct regions can be identified with respect to methane concentration:

- **Low methane region (2% - 4%)** The sp^3/sp^2 ratio increases slightly, peaking at around 4% of CH_4 and a similar trend is observed, with a slightly sharper peak at 4% CH_4. At low CH_4 concentrations, the environment favors the formation of sp^3 bonds. This may be due to the optimum balance of carbon to H-atoms to sustain tetrahedral bonds in a diamond structure. [8].
- **Medium methane region (4% - 8%)** Tthe sp^3/sp^2 ratio begins to decrease. A moderate increase in CH_4 leads to competition between sp^3 and sp^2 bond formation. Available carbon begins to form graphitic and other amorphous structures in addition to diamond bonds.
- **High methane region (8% - 12%)** The sp^3/sp^2 ratio decreases substantially. At high CH_4 concentrations, the formation of graphite and amorphous materials becomes predominant, with sp^2 bonds dominating, thereby reducing the sp^3/sp^2 ratio [38].

The above analysis clearly indicates that plasma chemistry that boosts amorphous carbon growth is detrimental to the growth of diamond nanoparticles. Of course, the plasma chemistry originating from hydrocarbon plasmas is much more complex.

4. Nucleation mechanism of nanodiamonds

The major question here is how the nanodiamonds nucleation could occur from the primary hydrocarbon species/ radicals on a pristine substrate devoid

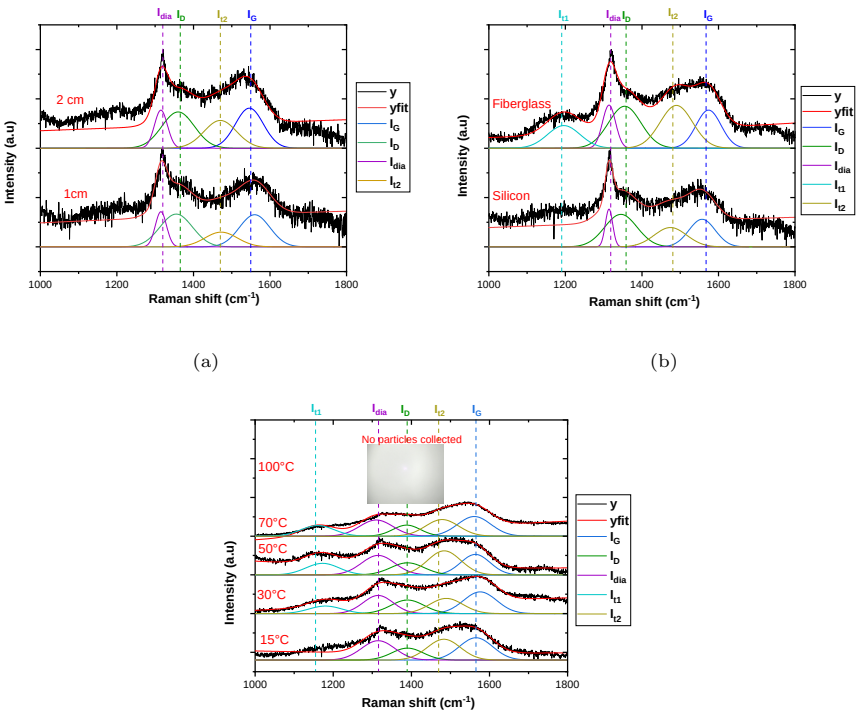

(a)

(b)

(c)

Figure 5: Raman spectra for different (a) plasma-substrate distances, (b) different type of substrate and (c) different substrate temperature. Experimental conditions: CH_4 = 4 sccm, H_2 = 96 sccm, Pressure = 100 mbar, power = 90W and deposition time : 1h.

of any active carbon site. Carbon phase diagram indicates that diamond can be only stable at high pressures and high temperature conditions. Moreover, nanodiamonds are only stable for sizes less than 10 nm at low pressure conditions. The formation of nanodiamonds at low pressure can only be explained by the metastable conditions that accompany the conditions.

Substantial amount of studies has focussed on nucleation and growth of diamond on a [39]. Nucleation of diamond on a substrate is extremely challenging due to the high surface energy associated with diamond, and it would be difficult to nucleate diamonds without surface pre-treatment on most materials [39]. The key factor that supports growth of diamond phase is the good concentration of H-atoms and CH_3 radicals where the methyl radical would attach to the existing active carbon sites on the substrate and H-atom stabilizing the sp^3 phase by etching the sp^2 phase. The collection of carbon nanostrucutres on the silicon substrate is very sensitive to substrate temperature. The substrate temperature in the above experiments were no more than 50 $^{\circ}C$. Also, the gas temperature measured at about 5 mm downstream of the plasma was close to room temperature [37]. Nucleation and growth of diamond phase on a substrate is much easier at substrate temperatures > 600 K [11] and the conditions in our experiments are not ideal for nucleation and growth of nanodiamonds on the surface.

For the matter of fact, one could observe nanodiamond phase in carbon nanostructures collected directly on a carbon TEM grid within 5 minutes of deposition (c.f. Figure 2c). Of course, it can be argued that carbon grid may have served as nucleation sites for diamond growth. Therefore, deposition were performed on different pristine untreated silicon and fiberglass substrates. The corresponding Raman spectra (Figure 5b) show that the signature of the carbon nanostructures produced was insensitive to the nature of the substrate. Furthermore, the distance between the silicon substrate and plasma discharge was varied within a range of 1 to 2 cm (Figure 5a). Although the density of NPs deposited on the surface decreased with distance, the Raman spectra signatures remained consistent across distances, suggesting that the proximity of

the substrate to the plasma did not significantly alter the characteristics of the carbon nanostructures formed.

However, it is quite possible that larger molecules of hydrocarbons may have been formed in the gas phase and deposited on the substrate, which act as sites for subsequent growth of carbon nanostructures. Having said that, the concentration of radicals such as CH_3 and to certain extent H-atom density at the substrate surface is expected to decrease substantially with distance as seen from H-atom density measurements reported in Siby et al. [37]. In addition, the conversion of methane to acetylene is very efficient. Acetylene based chemistry being sp^2 driven, the lack of H-atom densities at large distances to effectively etch the sp^2 phase formed on the carbon nanostructure should increase the yield of sp^2 phase carbon. On the contrary, there was no change in the quality of carbon nanostructures collected with distance and therefore, it could be concluded that surface based processes are not dominant.

In order to study the effect of substrate temperature, carbon nanostructures were collected on a substrate over a distance of 1 cm and 1 hour at different substrate temperatures: 15, 30, 50, 70 and 100°C and their Raman spectra are shown in Figure 5c. At 15 and 30°C, the Raman spectrum shows significant peaks for the diamond and graphite phases, indicating substantial nanoparticle collection. As the substrate temperature rises, there is a reduction in overall peak intensity due to lower density of deposited NPs. However, the quality of the deposit does not indicate an appreciable change. At 70°C, there is hardly any deposit and the Raman intensities were greatly reduced with consistent presence of Diamond peak. No particles were collected on the silicon substrate at temperatures greater than 100°C. The effect of substrate temperature can be twofold. Firstly, it would have profound effect of the gas cooling on the downstream of the plasma and therefore could alter the gas chemistry that in turn impact the chemistry at the surface of the substrate. Secondly, if the NPs are indeed nucleated in the gas phase, the temperature gradient close to the substrate can influence their collection as a result of thermophoretic forces. At higher temperatures, the thermophoretic force drives nanoparticles away from

the hot substrate, reducing the likelihood of their deposition. This effect becomes more pronounced with increasing temperature, contributing to the decrease in nanoparticle collection observed at 50°C and 70°C, and the absence of carbon nanostrucutres at 100°C. Furthermore, the decrease in NP density with distance is consistent with the hydrodynamics of stagnation flow, where the radial diffusion of nanoparticles increases with distance and hence reduces the collection of nanoparticles.

Figure 6a illustrates the Raman spectra of carbon nanostructures collected on a silicon substrate over different deposition durations, ranging from 5 to 60 minutes. The similarity in the Raman spectral signatures of diamond, D-Band, G-Band and Transpolyacetylene peaks across these time intervals indicates that the fundamental characteristics of the carbon nanostructures were established early in the deposition process and did not significantly evolve with longer deposition times. Moreover, SEM images indicate the nucleation of nanoparticles without any formation of films, even after 1 hour of deposition. Unless carbon can nucleate on a silicon substrate, the results indicate a probable nucleation of carbon nanostructures in the gas phase. This can be further confirmed by the evolution of particle size density and average particle size over deposition time, as shown in Figure 6b. The particle density increases with time, with the average particle size hovering around 10 nm for all depositions. The minimal evolution of particle size on the substrate is indicative that growth of the deposited carbon nanostructures by surface reactions are limited and hence do not significantly modify the Raman signature of the carbon nanostructures. These observations suggest that nucleation predominantly occurs in the gas phase rather than being heavily influenced by the substrate conditions, which is much more critical for growth of CVD diamond crystals and films[38, 40].

Gas phase based process of nucleation of carbon nanostructures relies on creation of primary hydrocarbon radicals that further grow to form larger molecules that eventually lead to nucleation of nanoparticles. The chemistry of hydrocarbons is strongly intertwined with atomic hydrogen and gas temperature. Gas temperature and H-atom density have been measured using ps-TALIF, details

of which are provided in Siby et al.[37]. Emission from C_2 Swann and CH A-X systems were also recorded and serve as a measure of relative density of the respective molecules. Figure 7a shows the variation of gas temperature and H-atom density as a function of pressure. Note that the gas temperature was measured for a pure hydrogen plasma, while the H-atom density is averaged over various methane concentrations at a specified pressure. The gas temperature increases with pressure for the same injected power. The effect of pressure is two folds. Firstly, the plasma volume would decrease with increase in pressure, which would result in an increase in electron density. As a result, the electron impact process increases and the dissociation of H_2 increases, as evident in the increase in the H-atom density. Further, the gas temperature too would increase due to increased thermalization due to higher collisional frequencies at higher pressure. The increase in gas temperature could graphitize the diamond phase leading to lower yield of diamond phase.

The coupling between H-atoms and early hydrocarbons are summarized in Figure 9. Formation of key radicals CH_3, CH are formed due to H-shift reactions on CH_4. High concentrations of H-atom will favor strong reduction of CH_4 towards radicals such as CH_3 or even highly reactive C radical. Furthermore, the other key radical C_2 are also readily formed from C and CH radicals as well as reduction of C_2H by H-atoms. The H-atom density is almost constant over the methane concentration at a fixed pressure. The linear increase of radicals C_2 and CH at small concentrations of methane are indicative of increase in methane concentration. However, the saturation of these radicals for $CH_4>$ 10% could indicate the net production of these radicals remain constant. This could be the relative density of H-atom not sufficient to shift the reduction of high concentration of CH_4 towards these radicals. In other words, key radicals such as CH_3 and C_2 do not increase in proportion in spite of the increase in CH_4. Global chemistry calculations for the conditions of the torch indicate that most of the hydrocarbons at the exit of the torch are converted to acetylene.

Correlating with the spectra of Raman, three prominent types of molecular growth pathways of carbon nanostructures can be identified. Soot comprising

aromatic compounds represented by G and D bands would be formed from intermediate poly-aromatic-hydrocarbons (PAHs) through mechanisms such as HACA [41]. The second molecular pathway should lead to the formation of linear unsaturated polyenes represented by Transpolyacetylene. These are often found in growth of nanocrystalline diamond and occur due to attachment of acetylene molecules and compounded by insufficient etching by H-atoms. The third molecular pathway representing sp^3 molecules remains elusive to the scientific community and remains an enigma. The only known mechanism known to the authors to date comes from Dolmatov et al. [1] where they discuss the formation of adamantine from C_2 radicals as the first critical step towards nucleation of nanodiamonds. Moreover, studies have demonstrated higher diamondoids can be formed when adamantine is directly introduced in a hydrocarbon plasma [42, 43] and this could possibly the route in our plasma as well. Figure 8 presents a Raman spectrum obtained for deposits made over a period of one hour with plasma conditions of 96% H_2 and 4% CH_4 at 100 mbar pressure and 90 W injected power, without external heating or polarization. Under these conditions, two distinct regions of deposits are observed depending on their proximity to the plasma torch: the outer region and the inner region (cf. Figure 8). The inner region, which is closer to the plasma and that can be visibly identified by the dark zone on the silicon substrate, shows peaks of the D, G, diamond and transpolyacetylene peaks. In fact, this region was the focus of all the Raman analyses reported so far in this work. However, one could also see deposits far from the influence of the plasma (about 1 cm away), referred to as outer region in the Figure 8 and visibly having grey coloration. This region had well-dispersed nps which should have been collected on the substrate due to the hydrodynamic drag. Their Raman signature shows several fine peaks associated with CH wag, CH_2 twist, and CH_2 scissor vibrational modes. These characteristics suggest the presence of nascent molecular structures that consist of CH_2 structures associated with sp^3 hybridized carbon as well as CH terminations associated with linear chains of sp^2 like polyacetylene. However, further studies were restricted by the sparse quantity of material collected. Nevertheless, these

molecular structures clearly provide evidence of molecular growth in gas phase and more chemical analysis of the plasma gas efflux using gas chromatography or mass spectrometer will reveal the key intermediary species and molecular growth pathways. This is currently being probed.

Theoretical studies show that nanodiamonds can be stable for sizes less than 10 nm in the conditions encountered [44, 45, 46]. Furthermore, the stability of nanodiamonds increase with H-termination [46] which could be the case of our experiments as well. The H_2 molecule and the H-atom should work in tandem in ensuring the nucleation, growth and stabilization of nanodiamond clusters. H-atom would be to take part in H-abstraction reactions that allows for creation of new active sites for carbon radicals present in the plasma to attach. The attachment of radicals such as CH_3, C_2 and C_2H allows for molecular growth. It can be ascertained that the H_2 molecule would saturate the different unsaturated hydrocarbon intermediaries and also ensure H-terminated clusters and NPs. As the amount of H-atoms do not change with concentration of methane, the increase in methane leads to increase in acetylene that in turn would lead to increase in unsaturated hydrocarbon molecules and decrease the degree of sp^3 molecules. Furthermore, H-atom are themselves consumed in the H-abstraction reactions of unsaturated molecular growth, as seen in the case of HACA mechanism involving acetylene to form PAHs. As a result, these alternate molecular pathways leading to amorphous structures would compete with sp^3 based growth mechanism and hence decrease the quantity of sp^3 hybridized nanoparticles. This is quite evident when the transpolyacetylene and disordered sp^2 phase grow strongly over the diamond phase with concentration of methane. In fact the sp^2 growth to form soot/transacetylene or even sp growth phase to form polyynes are common aspects of a H-deficient local conditions where the present plasma offers a condition with much higher concentrations of H-atom at moderate temperatures that allows for the highly latent sp^3 molecular growth to co-exist.

5. Conclusion

This paper examined the formation and properties of carbon nanostructures obtained from a CH_4/H_2 low-pressure-low temperature microplasma. The characterization revealed a hybrid composition made up of amorphous soot and transpolyacetylene and crystalline diamond phases, with nucleation occurring primarily in the gas phase. The particle size distribution ranged from 5 to 30 nm. Evidence suggest that nucleation occurs rapidly in the gas phase, with little role of the substrates. The abundance of nanodiamonds in the carbon nanostructures may be affected by the parallel molecular growth pathways that co-exist. This study demonstrated that the optimal conditions for high-quality nanodiamond synthesis using the MW-plasma torch with H_2/CH_4 gas precursors are a methane concentration of 4% and a pressure of 100 mbar at 90 W. The major conclusion of the paper is that nucleation of nanodiamonds can occur under high densities of H-atom while keeping optimum concentrations of hydrocarbon species. H-atom rich atmosphere is not only important for creation of key small radicals in the early phase of growth process but also important for molecular growth and nucleation of nanodiamonds during the later stages. The quality of nanodiamonds should also be influenced by the temperature, as it is likely that nanodiamonds will graphitize at higher temperatures. An critical factor to nucleate diamonds would be to restrict the alternate growth pathways, either through growth of PAHs or polyacetylene structures that are promoted by acetylene. Increase in hydrocarbon species would tilt the balance towards growth of sp_2 and amorphous carbon nanostructures.

Acknowledgement

This work was funded by the French Agence Nationale de la Recherche (ANR), under grants ANR-22-CE51-0013 (project NANODIAPLAS) and ANR-22-CE51-0027-02 (project ULTRAMAP), Labex SEAM (ANR-10-LABX-0096; ANR-18-IDEX0001, LA01PRASAN233690LSPMXR) and IDF regional project

SESAME DIAGPLAS. One of the authors (Khaled Hassouni) acknowledges the support of the Institut Universitaire de France.

References

[1] V. Y. Dolmatov, A. N. Ozerin, I. I. Kulakova, O. O. Bochechka, N. M. Lapchuk, V. Myllymäki, A. Vehanen, Detonation nanodiamonds: new aspects in the theory and practice of synthesis, properties and applications, Russ. Chem. Rev. 89 (12) (2020) 1428.

[2] J. Narayan, A. Bhaumik, Novel phase of carbon, ferromagnetism, and conversion into diamond, Journal of Applied Physics 118 (21) (2015).

[3] S. Kumar, M. Nehra, D. Kedia, N. Dilbaghi, K. Tankeshwar, K.-H. Kim, Nanodiamonds: Emerging face of future nanotechnology, Carbon 143 (2019) 678–699.

[4] A. K. Khachatryan, S. Aloyan, P. May, R. Sargsyan, V. Khachatryan, V. Baghdasaryan, Graphite-to-diamond transformation induced by ultrasound cavitation, Diamond and Related Materials 17 (6) (2008) 931–936.

[5] V. A. Davydov, A. V. Rakhmanina, S. Lyapin, I. D. Ilichev, K. N. Boldyrev, A. Shiryaev, V. N. Agafonov, Production of nano-and microdiamonds with si-v and nv luminescent centers at high pressures in systems based on mixtures of hydrocarbon and fluorocarbon compounds, JETP letters 99 (2014) 585–589.

[6] E. Ekimov, K. Kondrina, N. Mordvinova, O. Lebedev, D. Pasternak, I. Vlasov, High-pressure, high-temperature synthesis of nanodiamond from adamantane, Inorganic Materials 55 (2019) 437–442.

[7] Z. Wang, Y. Zhao, K. Tait, X. Liao, D. Schiferl, C. Zha, R. T. Downs, J. Qian, Y. Zhu, T. Shen, A quenchable superhard carbon phase synthesized by cold compression of carbon nanotubes, Proceedings of the National Academy of Sciences 101 (38) (2004) 13699–13702.

[8] J. Robertson, Diamond-like amorphous carbon, Materials science and engineering: R: Reports 37 (4-6) (2002) 129–281.

[9] J. E. Butler, I. Oleynik, A mechanism for crystal twinning in the growth of diamond by chemical vapour deposition, Philosophical Transactions of the Royal Society A: Mathematical, Physical and Engineering Sciences 366 (1863) (2008) 295–311.

[10] S. Matsumoto, Y. Sato, M. Kamo, N. Setaka, Vapor deposition of diamond particles from methane, Japanese Journal of applied physics 21 (4A) (1982) L183.

[11] A. Gicquel, K. Hassouni, F. Silva, J. Achard, Cvd diamond films: from growth to applications, Current Applied Physics 1 (6) (2001) 479–496.

[12] D. M. Gruen, C. D. Zuiker, A. R. Krauss, X. Pan, Carbon dimer, c2, as a growth species for diamond films from methane/hydrogen/argon microwave plasmas, Journal of Vacuum Science & Technology A: Vacuum, Surfaces, and Films 13 (3) (1995) 1628–1632.

[13] O. A. Shenderova, A. I. Shames, N. A. Nunn, M. D. Torelli, I. Vlasov, A. Zaitsev, Synthesis, properties, and applications of fluorescent diamond particles, Journal of Vacuum Science & Technology B 37 (3) (2019) 030802.

[14] J. Achard, V. Jacques, A. Tallaire, Chemical vapour deposition diamond single crystals with nitrogen-vacancy centres: a review of material synthesis and technology for quantum sensing applications, Journal of Physics D: Applied Physics 53 (31) (2020) 313001.

[15] R. S. Lewis, T. Ming, J. F. Wacker, E. Anders, E. Steel, Interstellar diamonds in meteorites, Nature 326 (6109) (1987) 160–162.

[16] J.-Y. Raty, G. Galli, Ultradispersity of diamond at the nanoscale, Nature Materials 2 (12) (2003) 792–795. doi:10.1038/nmat1018.

[17] J. B. Lewis, C. Floss, D. Isheim, T. L. Daulton, D. N. Seidman, R. Ogliore, Origins of meteoritic nanodiamonds investigated by coordinated atom-probe tomography and transmission electron microscopy studies, Meteoritics & Planetary Science 55 (6) (2020) 1382–1403. arXiv:https://onlinelibrary.wiley.com/doi/pdf/10.1111/maps.13373, doi:https://doi.org/10.1111/maps.13373.
URL https://onlinelibrary.wiley.com/doi/abs/10.1111/maps.13373

[18] T. Gries, L. Vandenbulcke, J. Rouzaud, S. De Persis, Diagnostics in dusty c–h–o plasmas with diamond and graphitic nanoparticle generation, Plasma Sources Sci. Technol. 19 (2) (2010) 025015.

[19] Z. Jia, Y. Fermi, A. Siby, O. Brinza, K. Hassouni, S. Prasanna, Enhanced gas-phase nucleation of diamond nanoparticles in a microplasma torch, Plasma Processes and Polymers 20 (3) (2023) 2200180.

[20] T. Nikhar, S. V. Baryshev, Evidence of gas phase nucleation of nanodiamond in microwave plasma assisted chemical vapor deposition, AIP Advances 14 (4) (2024).

[21] A. Kumar, P. Ann Lin, A. Xue, B. Hao, Y. Khin Yap, R. M. Sankaran, Formation of nanodiamonds at near-ambient conditions via microplasma dissociation of ethanol vapour., Nature communications 4 (2013) 2618. doi:10.1038/ncomms3618.
URL http://www.ncbi.nlm.nih.gov/pubmed/24141249

[22] S. Iqbal, M. S. Rafique, M. Zahid, S. Bashir, M. A. Ahmad, R. Ahmad, Impact of carrier gas flow rate on the synthesis of nanodiamonds via microplasma technique, Mater. Sci. Semicond. Process. 74 (2018) 31–41.

[23] M. Frenklach, R. Kematick, D. Huang, W. Howard, K. Spear, A. W. Phelps, R. Koba, Homogeneous nucleation of diamond powder in the gas phase, J. Appl. Phys. 66 (1) (1989) 395–399.

[24] M. Frenklach, W. Howard, D. Huang, J. Yuan, K. Spear, R. Koba, Induced nucleation of diamond powder, Applied physics letters 59 (5) (1991) 546–548.

[25] A. Sadezky, H. Muckenhuber, H. Grothe, R. Niessner, U. Pöschl, Raman microspectroscopy of soot and related carbonaceous materials: Spectral analysis and structural information, Carbon 43 (8) (2005) 1731–1742.

[26] A. K. Arora, T. Ravindran, G. Reddy, A. K. Sikder, D. Misra, Nature of confinement of phonons in nanocrystalline cvd diamond, Diamond and related materials 10 (8) (2001) 1477–1485.

[27] K.-W. Sun, J. Wang, T. Ko, Photoluminescence and raman spectroscopy of single diamond nanoparticle, Journal of Nanoparticle Research 10 (2008) 115–120.

[28] D. Bogdanov, A. Bogdanov, V. Plotnikov, S. Makarov, A. Yelisseyev, A. Chepurov, Core growth of detonation nanodiamonds under high-pressure annealing, RSC Advances 11 (21) (2021) 12961–12970.

[29] V. I. Korepanov, H.-o. Hamaguchi, E. Osawa, V. Ermolenkov, I. K. Lednev, B. J. Etzold, O. Levinson, B. Zousman, C. P. Epperla, H.-C. Chang, Carbon structure in nanodiamonds elucidated from raman spectroscopy, Carbon 121 (2017) 322–329.

[30] L. Hu, Y. Guo, S. Du, S. Tian, J. Li, C. Gu, Probing trans-polyacetylene segments in a diamond film by tip-enhanced raman spectroscopy, Diamond and Related Materials 116 (2021) 108415.

[31] A. Ferrari, J. Robertson, Origin of the 1 1 5 0- cm- 1 raman mode in nanocrystalline diamond, Physical review B 63 (12) (2001) 121405.

[32] R. Pfeiffer, H. Kuzmany, N. Salk, B. Günther, Evidence for trans-polyacetylene in nanocrystalline diamond films from h–d isotropic substitution experiments, Applied Physics Letters 82 (23) (2003) 4149–4150.

[33] K. Ganesan, P. Ajikumar, S. Srivastava, P. Magudapathy, Structural, raman and photoluminescence studies on nanocrystalline diamond films: Effects of ammonia in feedstock, Diamond and Related Materials 106 (2020) 107872.

[34] M. Veres, S. Tóth, M. Koós, Grain boundary fine structure of ultrananocrystalline diamond thin films measured by raman scattering, Applied Physics Letters 91 (3) (2007).

[35] B. Baudrillart, F. Bénédic, T. Chauveau, A. Bartholomot, J. Achard, Nanocrystalline diamond films grown at very low substrate temperature using a distributed antenna array microwave process: Towards polymeric substrate coating, Diamond and Related Materials 75 (2017) 44–51.

[36] T. Leung, W. Man, P. Lim, W. Chan, F. Gaspari, S. Zukotynski, Determination of the sp3/sp2 ratio of ac: H by xps and xaes, Journal of non-crystalline solids 254 (1-3) (1999) 156–160.

[37] A. Siby, D. Stefas, Y. Agha, L. Invernizzi, K. Gazeli, G. Lombardi, K. Hassouni, S. Prasanna, Gas temperature measurements from ps-talif in highly collisional plasmas, Physics of Plasmas 31 (3) (2024).

[38] A. C. Ferrari, J. Robertson, Interpretation of raman spectra of disordered and amorphous carbon, Physical review B 61 (20) (2000) 14095.

[39] S. Mandal, Nucleation of diamond films on heterogeneous substrates: a review, RSC advances 11 (17) (2021) 10159–10182.

[40] D. M. Gruen, Nanocrystalline diamond films, Annual Review of Materials Science 29 (1) (1999) 211–259.

[41] M. Frenklach, A. M. Mebel, On the mechanism of soot nucleation, Physical Chemistry Chemical Physics 22 (9) (2020) 5314–5331.

[42] S. Stauss, C. Ishii, D. Z. Pai, K. Urabe, K. Terashima, Diamondoid synthesis in atmospheric pressure adamantane–argon–methane–hydrogen mix-

tures using a continuous flow plasma microreactor, Plasma Sources Science and Technology 23 (3) (2014) 035016.

[43] C. Ishii, S. Stauss, K. Kuribara, K. Urabe, T. Sasaki, K. Terashima, Atmospheric pressure synthesis of diamondoids by plasmas generated inside a microfluidic reactor, Diamond and Related Materials 59 (2015) 40–46.

[44] M. Gamarnik, Size-related stabilization of diamond nanoparticles, Nanostructured materials 7 (6) (1996) 651–658.

[45] N. M. Hwang, J. H. Hahn, D. Y. Yoon, Charged cluster model in the low pressure synthesis of diamond, Journal of Crystal Growth 162 (1) (1996) 55–68. doi:10.1016/0022-0248(95)00943-4.

[46] A. S. Barnard, S. P. Russo, I. K. Snook, Modeling of Stability and Phase Transformations in Quasi-Zero Dimensional Nanocarbon Systems, Journal of Computational and Theoretical Nanoscience 2 (2) (2005) 180–201. doi:10.1166/jctn.2005.102.

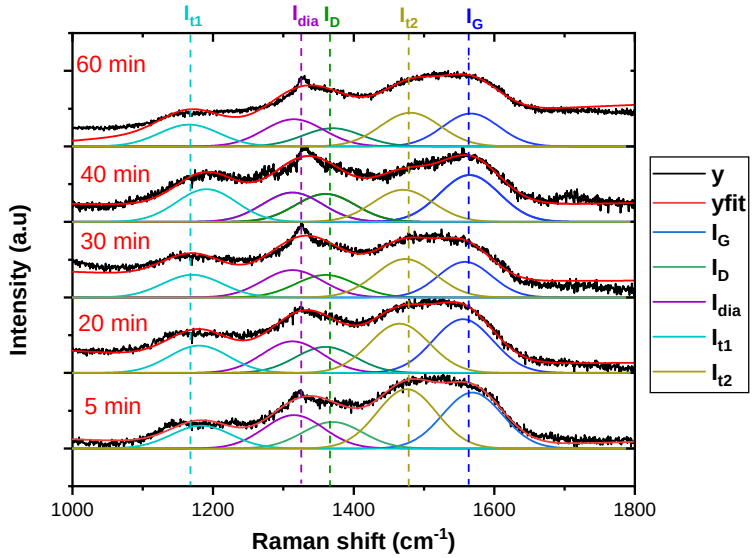

(a)

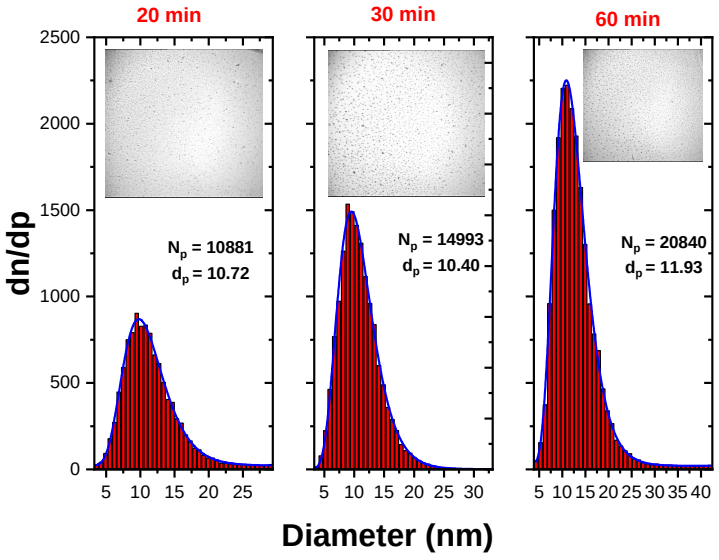

(b)

Figure 6: Raman spectra for different deposition time (a) and Particle size distribution for different deposition time (b). Insets of the respective images are shown.

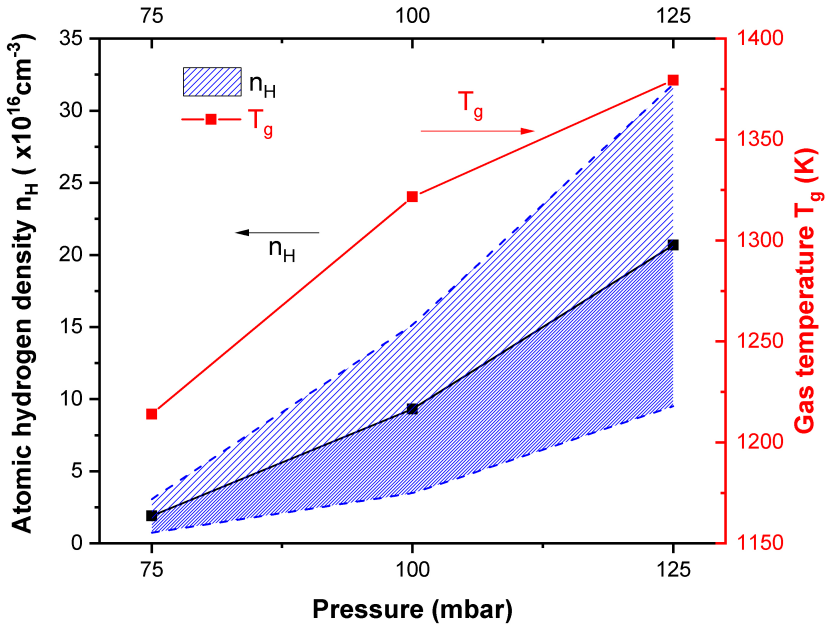

(a)

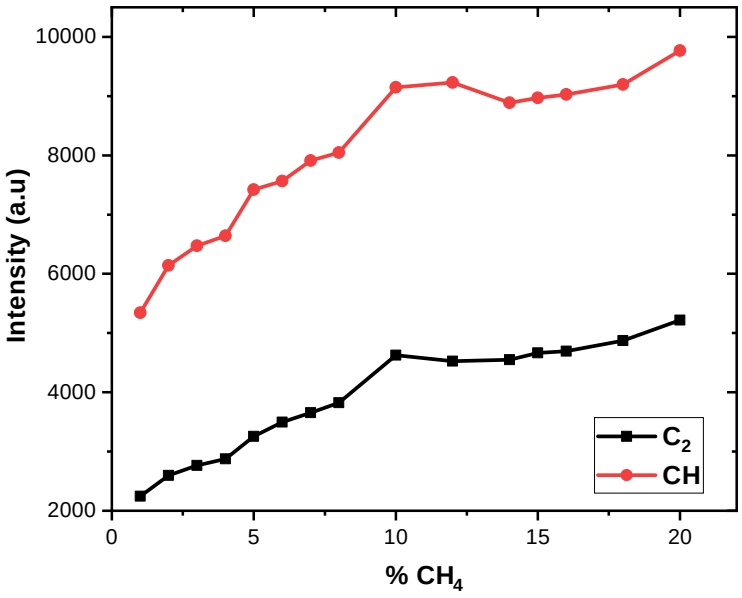

(b)

Figure 7: Evolution of (a) gas temperature and atomic hydrogen density as a function of different pressure at 90W ,(b) and relative densities of C_2 and CH inferred from emission of C_2 Swann and CH $A - X$ respectively as a function of CH_4 concentration at 100 mbar and 90W

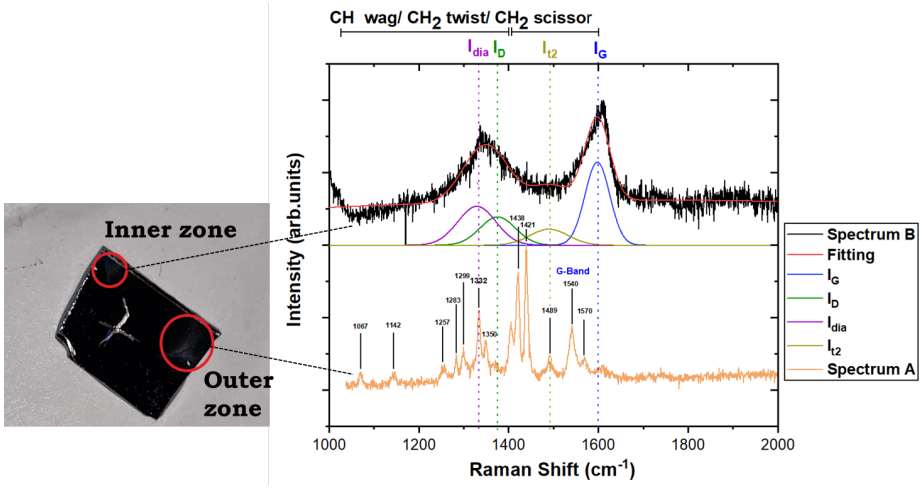

Figure 8: Raman spectra showing the two regions of deposition

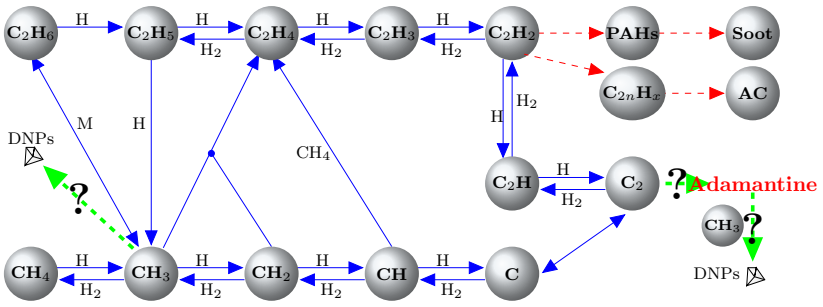

Figure 9: Reaction pathways of hydrocarbon chemistry starting from methane